

Room temperature molecular and lattice structures of a homologous series of anhydrous zinc(II) *n*-alkanoate

Richard A. Taylor, Henry A. Ellis*

Department of Chemistry, University of the West Indies, Mona, Kingston 7, Jamaica

Received 4 September 2006; accepted 9 November 2006

Abstract

The room temperature structures and lattice arrangements of a homologous series of zinc(II) *n*-alkanoates from chain length, $n_C = 4$ –20, inclusive, have been studied using infrared spectroscopy, X-ray diffraction and polarizing light microscopy. Lattice parameters from single crystal and powder diffraction data, for zinc(II) hexanoate, are compared to validate the use of the powder method. Since they are in excellent agreement, the powder data are analyzed by a software programme to determine lattice parameters for all the homologues. These are used, in conjunction with infrared, X-ray, density and molecular model calculations to determine molecular and lattice structures. The compounds are isostructural, in that, each zinc atom is tetrahedrally coordinated to oxygen atoms from four different carboxylate groups and each ligand forms a *Z,E*-type bidentate bridge with two tetrahedral zinc atoms resulting in a *syn-anti* arrangement. The hydrocarbon chains are in the fully extended all-trans configuration and are tilted at an average angle of 60° to the zinc basal plane. For the short chain length compounds with $n_C \leq 8$, a double bilayer in-plane-perpendicular-perpendicular-in-plane arrangement of hydrocarbon chains, with two molecules per unit cell, is indicated. For the others, an interdigitating in-plane-in-plane bilayer with head-to-tail interactions, with one molecule per unit cell, is proposed. A geometric model is presented to account for odd–even chain effects and to explain the differences in melting points and densities between these adducts. All the compounds crystallize in the monoclinic space group with *P* symmetry and are arranged in a two-dimensional network along the *ac* plane within the unit cell.

© 2006 Elsevier B.V. All rights reserved.

Keywords: Zinc(II) *n*-alkanoates; Infrared spectroscopy; X-ray diffraction; Polarizing light microscopy; Lattice parameters; Densities

1. Introduction

In a previous publication [1], room temperature molecular and lattice structures were proposed for anhydrous zinc(II) hexanoate and pentadecanoate. Infrared and X-ray diffraction studies pointed to *syn-anti* bridged structures, with the zinc atom coordinated to oxygen atoms from four different carboxylate groups; a result in excellent agreement with other published molecular structures of these long chain compounds [2–6]. However, there have been few systematic studies on the effect of hydrocarbon chain length on the lattice structures and chain packing within a unit cell. At least for the hexanoate and pentadecanoate, hydrocarbon chains are packed within lamellae and tilted at an average angle of 60° to the zinc basal plane [1]. Additionally, they crystallize within a monoclinic unit cell with

P1c1 and *P* symmetry, respectively. One complicating factor is that the long chain compounds are of such low symmetry that it is difficult to grow single crystals from them for X-ray studies. Another is the presence of polymorphic forms of these structures arising, in part, from their methods of synthesis and other unknown factors. These are characterized by hydrocarbon chains interacting or orientated differently in the various lattices. For example, Segedin et al. [5], on the basis of infrared, X-ray diffraction and solid state ^{13}C NMR studies, demonstrated the presence of polymorphic structures for zinc(II) hexanoate and heptanoate though they did not report structures for them. Indeed, a definitive picture of the molecular units within the lattice has not been reported, except for a few short chain length compounds [4,7–10].

In this paper, the evolution of the structural properties of anhydrous zinc(II) *n*-alkanoate, $\text{Zn}(\text{C}_n\text{H}_{2n-1}\text{O}_2)_2$, containing 4–20 carbon atoms ($n = 4$ –20) inclusive, is studied in relation to the number of carbon atoms in the hydrocarbon chain and whether the chains contain an odd or even number of carbon

* Corresponding author. Tel.: +876 9271910; fax: +876 9771835.
E-mail address: henry.ellis@uwimona.edu.jm (H.A. Ellis).

atoms. This should give some insight in to the relationship between hydrocarbon chain length, molecular and lattice structures.

2. Experimental

The compounds were prepared by refluxing zinc oxide with an excess of the appropriate carboxylic acid in ethanol for approximately 2 h. The plate-like crystals, which precipitated, on cooling, were filtered off, washed with ethanol, repeatedly, collected and kept over silica gel in a vacuum desiccator (yield ~85%). The compounds were white microcrystalline solids. They were very thin ~150–200 μm and lath-like in shape with vertical cleavage. When viewed under polarized light, they exhibited pleochroism (displayed faint colour changes as the microscope stage was rotated), were anisotropic (birefringent values in the region of 0.003–0.004) and first order grey. Zinc(II) hexanoate single crystals were prepared as described previously [1].

The melting points of the compounds were determined by the capillary melting technique and differential scanning calorimetry (DSC). DSC melting points were determined using a Mettler TC 10A Processor attached to a DSC 20 standard cell. Between 3 and 10 mg of powder samples were sealed in standard aluminium pans with pierced lids and heated at a rate of 2 K/min over a temperature range of 323–353 K. Each run was performed in triplicate.

Infrared (IR) spectra were recorded in KBr pellets, at room temperature, on a Perkin-Elmer FTIR 1000 spectrometer over the range of 4000–400 cm^{-1} .

Single crystal diffraction measurements were carried out on a Bruker AXS P4 Diffractometer with Mo $\text{K}\alpha$ radiation ($\lambda = 0.71073$). Cell parameters were collected in a 2θ range of 9.7–25° and refined from 2494 reflections. The data were reduced by SHELXTL [11] and the structure refined and solved by SHELXS 97 [12]. ORTEP 3 [13] was the graphics programme used.

Powder diffraction data were collected, at room temperature, on a Bruker D5005 diffractometer with nickel filtered Cu $\text{K}\alpha$ radiation ($\lambda = 1.54056 \text{ \AA}$) from ungrounded samples mounted in standard plastic holders. The X-ray tube was operated at 45 kV and 35 mA at a time/step of 2 s for 2 h between 2° and 60°. Longer runs did not improve the diffraction patterns.

Microscopic studies were performed on samples mounted between glass slides and coverslips, using a Swift polarizing light microscope. For conoscopic studies, both slide and coverslips were pre-treated with an aqueous solution of 0.2% PVA, heated to approximately 373 K, for a few minutes, and cooled to ambient temperatures to produce good homeotropic textures for examination.

The densities of the compounds were determined by flotation in heptane/carbon tetrachloride mixtures.

3. Results and discussion

Elemental analyses of carbon and hydrogen of the synthesized compounds are given in Table 1. Since there is excellent

Table 1
Elemental analyses for anhydrous zinc(II) *n*-alkanoates

Compound	Carbon (%)		Hydrogen (%)	
	Experimental	Calculated	Experimental	Calculated
ZnC ₄	44.94	40.11	7.06	5.89
ZnC ₅	44.45	44.89	6.96	6.78
ZnC ₆	49.09	48.75	7.82	7.50
ZnC ₇	51.92	51.94	8.43	8.09
ZnC ₈	54.30	54.63	8.93	8.60
ZnC ₉	57.18	56.92	9.51	9.02
ZnC ₁₀	58.04	58.89	9.73	9.39
ZnC ₁₁	59.84	60.61	10.09	9.71
ZnC ₁₂	61.88	62.13	10.43	9.99
ZnC ₁₃	63.42	63.47	10.71	10.24
ZnC ₁₄	64.31	64.66	10.82	10.46
ZnC ₁₅	65.73	65.73	10.66	10.66
ZnC ₁₆	66.33	66.70	11.32	10.84
ZnC ₁₇	66.49	67.58	11.08	11.07
ZnC ₁₈	65.90	68.38	11.35	11.16
ZnC ₁₉	67.63	69.11	11.65	11.29
ZnC ₂₀	68.84	69.79	11.80	11.42

agreement between experimental and calculated values, it is reasonable to conclude that the compounds are of high purity.

Capillary and DSC melting points, in addition to density data, are given in Table 2. The sharp, final endothermic transition observed in the DSC trace is taken as the true melting point. Clearly, the capillary and DSC data are in good agreement though their values are consistently higher than the corresponding literature values. This is not surprising since, in the early literature, the melting points of these long chain soaps were collected, for the most part, from impure compounds. For example, basic $(\text{M}(\text{OH})_x(\text{RO})_2)$ and or acid soaps $(\text{RCO}_2)_x(\text{M}(\text{RO}_2\text{H}))$ are well-known contaminants. In some cases, using the capillary method, a high temperature phase transition was sometimes mistaken for the melting point [15].

Both melting point and density data, as a function of chain length, n_C are shown in Fig. 1. Both values decrease with increasing n_C . An odd–even effect, with increasing n_C , is observed for $n_C \geq 9$ with the values being somewhat higher for the even-chain length compounds. Odd–even melting behaviour in *n*-alkanes and other *n*-alkane derivatives is not unusual and has been studied quite extensively by Boese et al. [16,17]. They accounted for the effect by suggesting different packing arrangements of hydrocarbon chains in a crystal lattice. A geometric model, adapted from those workers, is presented here to explain the different packing arrangements for $n_C \geq 9$. The even and odd chains are fitted to a parallelogram (Fig. 2B) and trapezoid (Fig. 2F), respectively. The stacking of the methylene, methyl and carboxylate groups are the important factors here. For both odd and even chains, methylene groups are inter-grooved into adjacent chains above and below them and the terminal methyl groups are arranged in a staggered conformation but anti-parallel to neighbouring chains along the same plane. If the models are stacked on top of each other, as shown in Fig. 2C and G, then the same volume of void spaces for both even and odd chain are obtained. This would mean that they are of similar densities and hence melting points. This is clearly not in accord with the experimental results.

Table 2
Density and melting point data for zinc(II) *n*-alkanoates

Compound	Visual melting point (°C)		DSC melting point (± 0.2 °C)		Density (g cm^{-3})
	This study	Literature [14]	This study	Literature [14]	
ZnC ₄	156–157	–	158.5	–	1.36
ZnC ₅	154–156	–	157.9	–	1.35
ZnC ₆	145–147	141–143	149.9	144	1.30
ZnC ₇	140–142	–	142.9	–	1.24
ZnC ₈	140–141	135–137	141.4	132	1.19
ZnC ₉	134–137	–	138.4	–	1.12
ZnC ₁₀	137–138	128–130	138.8	131	1.14
ZnC ₁₁	135–137	–	135.2	–	1.10
ZnC ₁₂	133–135	127–130	134	127	1.09
ZnC ₁₃	135–136	–	134.3	–	1.07
ZnC ₁₄	132–134	126–128	133.2	125	1.08
ZnC ₁₅	132–133	–	130.3	–	1.05
ZnC ₁₆	133–135	126–128	133.8	123	1.06
ZnC ₁₇	132–133	–	131.2	–	1.05
ZnC ₁₈	135–136	124–126	134.2	121	1.06
ZnC ₁₉	134–135	–	131.8	–	1.04
ZnC ₂₀	136–136	–	134.8	–	1.05

However, as these units stack in a geometrically allowed manner (with an off-set to the right) aided by the conformation of the terminal methyl groups, the even-chain length lattice has few void spaces (Fig. 2D). This results in a high packing efficiency and high density. The odd chains are stacked in a manner that result in increased void spaces between the molecular units resulting in a lower packing efficiency and lower density (Fig. 2H).

Consequently, the more densely packed even-chain length compounds will have a higher melting point than the less densely packed odd chain length ones. Also, the overall decrease in melting point with increasing n_C may be ascribed to the energetics resulting from competition between zinc–carboxylate binding, which is favoured in the lower chain length compounds, and van der Waals interaction between hydrocarbon chains, which is a weaker force, and predominates in the longer chain length compounds.

4. Infrared spectroscopy

Infrared spectroscopy of long chain metal carboxylates provides information on metal carboxylate coordination, chain conformation and packing [18–20]. Thus, representative spectra, collected between 4000 and 400 cm^{-1} , at room temperature, are shown in Fig. 3. The spectra are characterized by strong absorptions in the region of 1700–1200 cm^{-1} and weak to medium bands between 1400 and 500 cm^{-1} . The regular progression of narrow bands, especially pronounced for short chain length compounds, between 1400 and 700 cm^{-1} , are assigned to the methylene progressive bands, typical for these compounds [21–23]. The absence of a carbonyl absorption band in the region of 1730 cm^{-1} and its replacement by carbonyl absorptions in the region of 1500, 1400, 950, 580 and 540 cm^{-1} indicates that there is complete resonance in the C–O bonds of the carbonyl group as a result of coordination between zinc and carboxylate ion; as well as the absence of free acid. Further, the absence of hydroxyl absorption bands in the region of 3500–3300 cm^{-1} confirms that the compounds are indeed anhydrous. The carbonyl bands are assigned as: the antisymmetric stretch, $\nu_a(\text{COO}) \sim 1538\text{--}1531 \text{ cm}^{-1}$; symmetric stretch, $\nu_s(\text{COO}) \sim 1409\text{--}1394 \text{ cm}^{-1}$; deformation, $\nu_d(\text{C–C})\text{COO} \sim 949\text{--}957 \text{ cm}^{-1}$; bending, $\nu_8(\text{COO}) \sim 745\text{--}743 \text{ cm}^{-1}$; out of plane twisting, $\nu_7(\text{COO}) \sim 580 \text{ cm}^{-1}$ and rocking, $\nu_p(\text{COO}) \sim 550\text{--}547 \text{ cm}^{-1}$. The $\nu_a(\text{COO})$ and

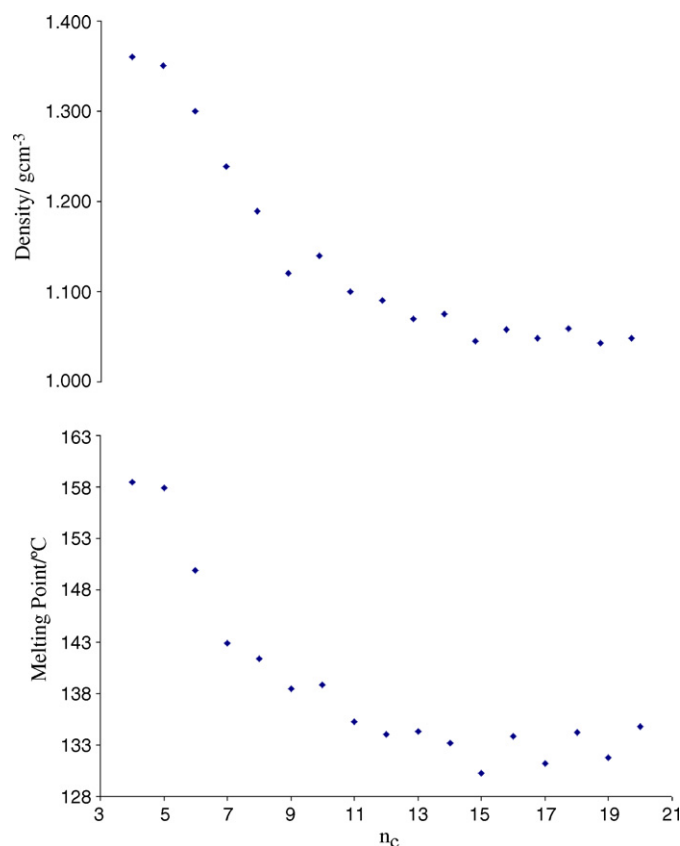


Fig. 1. Density and melting point vs. n_C .

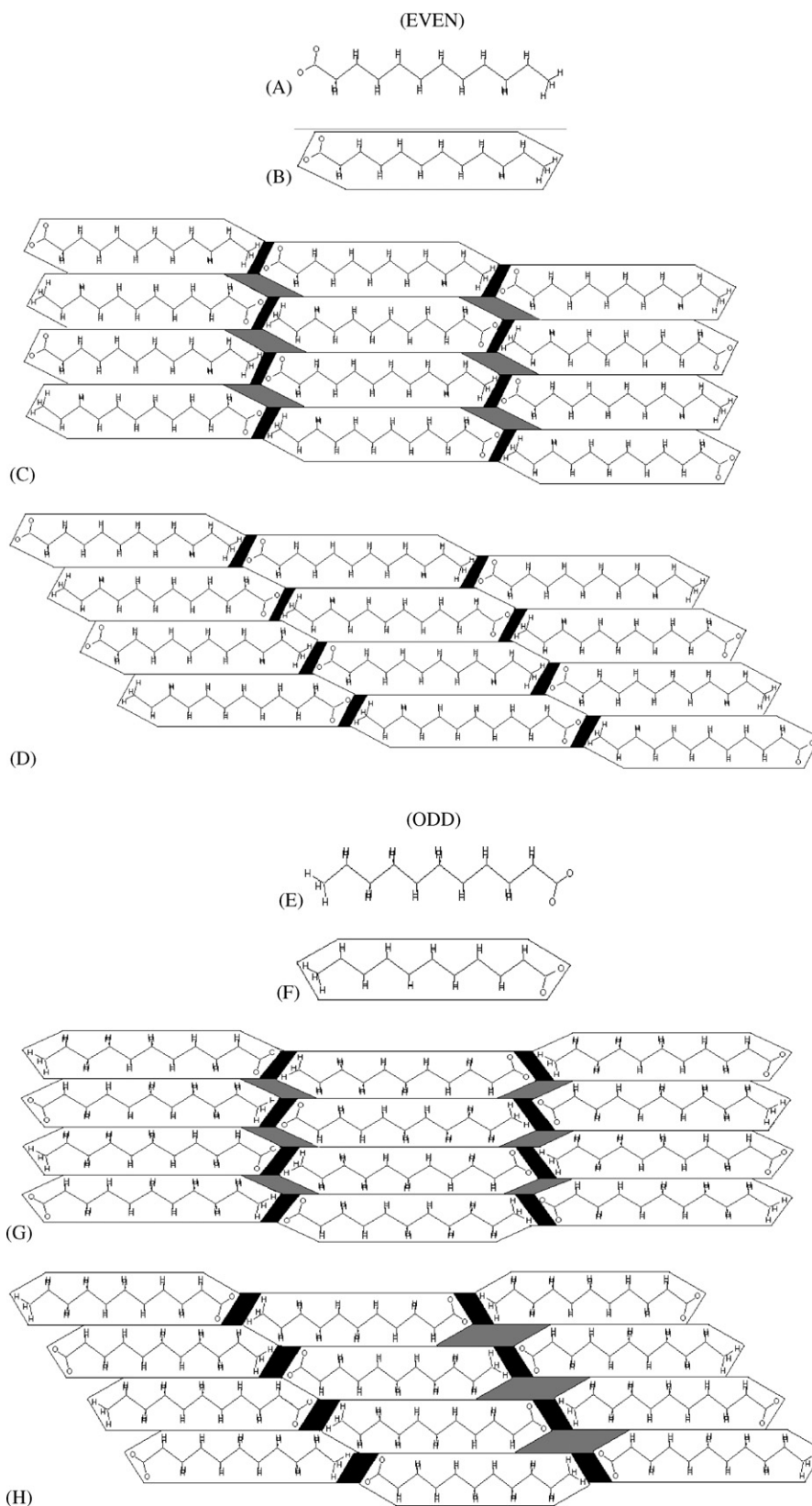


Fig. 2. Proposed geometrical models for $n_C \geq 9$ for even, A and B and odd, E and F chain length compounds. B and F are the parallelogram and trapezoid, respectively. C–H are the various packing arrangements. C and G represent intermediate packing when the terminal groups are not properly orientated. The dark lines are the void spaces. D and H represent the off-set packing arrangement.

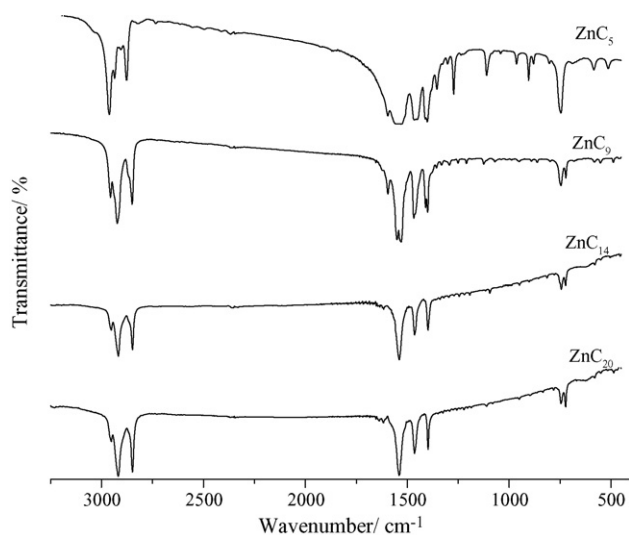


Fig. 3. Room temperature infrared spectra for ZnC_5 , ZnC_9 , ZnC_{14} and ZnC_{20} .

$\nu_s(\text{COO})$ absorptions are very strong bands in the regions of 1542–1530 and 1401–1397, respectively, for the entire homologous series. Interestingly, both are doublets for $n_C = 4$ –9 and singlets for $n_C > 10$ (Table 3). The splitting of these degenerate modes correlates with a lowering of symmetry and the relative strengths of the zinc–carboxylate bond and van der Waals interactions between hydrocarbon chains. It is expected that zinc–carboxylate binding will be favoured for short chain homologues, resulting in a stronger interaction between metal and ligand leading to splitting of these absorptions. For the long chain length homologues, there is no corresponding splitting as the metal–ligand bond becomes progressively weaker with increasing n_C , while van der Waals interchain interactions become progressively stronger. Ellis et al. [1–6] have provided conclusive evidence, from infrared, X-ray and other studies for bridging bidentate coordination as the mode of bonding for these com-

pounds. Each zinc atom is tetrahedrally coordinated to oxygen atoms from four different carboxylate groups and each ligand forms a *Z,E*-type bidentate bridge with two tetrahedral zinc atoms resulting in a *syn-anti* arrangement. Since the $\nu_a(\text{COO})$ and $\nu_s(\text{COO})$ absorptions are of unequal intensities throughout, because of the difference in zero-point energies between the asymmetric and symmetric modes, it implies that the C–O bonds coordinated to zinc are non-equivalent; that is, Zn–O bond lengths are not equal and, therefore, bonding around zinc is asymmetrical. Moreover, the near invariance of the $\rho(\text{COO})$ absorption in the region of 550–547 cm^{-1} supports a similar molecular structure for all the homologues. Any significant differences in frequency in this absorption would point to a change in molecular structures [3]. This is supported by the $\Delta\nu$ data collected in Table 3, where the values are in the right range for bridged structures [22–25]. Additionally, for triclinic or hexagonal chain packing, a single band for $\rho(\text{CH}_2)$ is expected; splitting of this band is indicative of orthorhombic or monoclinic packing [3,26]. In the present case, the band is a doublet, except for butanoate and pentadecanoate, and indicates that the compounds crystallize within a monoclinic or orthorhombic crystal system. These appear to be the preferred crystal systems. For example, Peultier et al. [9,10] reported an orthorhombic system for anhydrous zinc(II) heptanoate and a monoclinic one for anhydrous zinc(II) octanoate; hinting at a possible chain length dependence. Moreover, in these long chain compounds, hydrocarbon chains are usually packed in small periodic structures (subcells) within the unit cell. There are two possible types of subcells, depending on the lateral packing of the chains. The nature of the packing can be inferred from $\rho(\text{CH}_2)$ and $\delta(\text{CH}_2)$ absorption bands. If these bands are split, horizontal packing is indicated; if not, parallel packing is assumed [3]. In this case, there is no correlation split in the bands and so lateral packing is of the parallel-type. Further, the progression of regularly spaced absorptions, in the region of 1347–1232 cm^{-1} , arising from the wagging vibrations of methylene groups, are typical for aliphatic chains and

Table 3
Frequencies of main bands and COO separation (cm^{-1}) for Zn(II) *n*-alkanoates

Compound	Frequency of main bands and COO^- separation (cm^{-1})				
	$\nu_{as}(\text{COO})$	$\nu_s(\text{COO})$	$\Delta\nu$	$\rho(\text{CH}_2)$	$\rho(\text{COO})$
ZnC_4	1549/1532	1411/1401	131	744/736	547
ZnC_5	1549/1535	1410/1401	134	744/736	547
ZnC_6	1547/1531	1409/1399	132	743/727	547
ZnC_7	1549/1533	1409/1400	133	747/723	545
ZnC_8	1550/1530	1408/1398	132	747/723	551
ZnC_9	1550/1530	1410/1400	130	746/722	552
ZnC_{10}	1537	1397	140	745/722	548
ZnC_{11}	1534	1399	135	747/721	553
ZnC_{12}	1542	1397	143	743/723	549
ZnC_{13}	1537	1398	139	745/722	554
ZnC_{14}	1539	1398	141	744/723	551
ZnC_{15}	1538	1397	141	745/723	550
ZnC_{16}	1539	1398	141	743/723	550
ZnC_{17}	1539	1397	142	743/723	550
ZnC_{18}	1538	1398	140	744/723	550
ZnC_{19}	1539	1397	142	744/723	550
ZnC_{20}	1539	1397	142	745/723	550

indicate all-trans conformation of hydrocarbon chains in these structures.

5. X-ray diffraction

Details of the single crystal data and structure refinements, for anhydrous zinc(II) hexanoate, are given in a previous paper [1]. There are two crystallographically different zinc atoms, Zn(1) and Zn(2) as shown in Fig. 3. The Zn(1)–O bond (1.972(3) Å) is slightly longer than Zn(2)–O (1.947(3) Å), which points to unsymmetrical bonding around zinc, as indicated by the infrared data. Also, the results confirm that the chains are in the fully extended all-trans conformation. Although Segedin et al. [5] pointed to the presence of a polymorphic structure for this compound, they did not report a possible structure for it. Since their compound crystallized in the monoclinic space group, $P2_1/c$ and this in $P1c1$, it is not unreasonable to propose our structure as a polymorph. This proposal is confirmed, at least for $n_C \leq 9$ by the small difference in structure, when compared with $n_C \geq 9$, of the strong band centered at $\sim 1460 \text{ cm}^{-1}$ corresponding to antisymmetric methyl absorptions and scissoring modes for methylene group absorptions. A close examination of Fig. 4 shows that the hydrocarbon chains, in the plane of the paper, are parallel to each other along a zinc plane and perpendicular to the plane on the other side of the zinc atom. Conoscopic studies support this arrangement of chains within the lattice. For example, under polarized light two cleavage planes are observed, perpendicular to each other, most probably resulting from this type of lattice arrangement. Moreover, on rotating the microscope stage a biaxial interference figure is obtained. This is clear evidence for tilted hydrocarbon chains. In fact, molecular models indicate that the chains are tilted at an average angle of 60° , in good agreement with previous studies [9,10]. Indeed, the evidence for tilting of hydrocarbon chains in metal carboxylate compounds is overwhelming [24,27,28]. Additionally, two cleavage planes are observed, perpendicular to each other, most probably as a result of the *syn-anti* arrangement of chains within the lattice. Thus, the chains are packed: in-plane-perpendicular-perpendicular-in-plane (Fig. 4) throughout the whole lattice structure. The unit cell, for this short chain homologue, contains two molecules ($Z=2$) and is defined by the distance between two Zn(1) or Zn(2)

planes. Clearly, there are four hexanoate ligands within a unit cell. For the longer chain length compounds, no suitable crystal could be found for single crystal X-ray diffraction or conoscopic studies. For these, the compounds are analyzed by X-ray powder diffraction.

Typical powder patterns, collected at room temperature, are shown in Fig. 5 as intensity of the diffractive ray versus angle of diffraction, 2θ for ZnC₅, ZnC₁₂ and ZnC₂₀. No visible reflections are observed beyond a 2θ of 60° . The patterns are characterized by evenly spaced reflections throughout for those compounds with $n_C = 4-8$, as shown by the pattern for ZnC₅. However, the patterns for $n_C \geq 9$ are somewhat different, as shown by that for ZnC₂₀, where evenly spaced reflections are observed only at low angles; with those at intermediate and higher angles being irregularly spaced and of low intensity. The patterns in the low angle region are typical for reflections from a lamellar structure [23,25–27]. Since there are different patterns for the short and long chain compounds, in the region of $20^\circ \leq 2\theta \leq 25^\circ$, associated with side chain packing, suggest that the packing of hydrocarbon chains within the lamellae are not the same for these adducts.

Profile analyses are performed on powder patterns where peaks are chosen based on intensity and shape using Diffrac^{plus} EVA V.9.0 software (a part of the machine operating system) and are subsequently converted using the same software to a line profile appropriate for auto-indexing. The lines are auto-indexed using commercially available Win-Metric LS V. 2.1 for windows at a tolerance of <0.1 and subsequently refined at a tolerance in the region of 0.06 with figures of merit, $F_N \sim 13$ and $M_{20} \sim 19.0$. Most lines are completely single indexed except the very low intensity ones which are few. To validate the procedure, the powder lattice parameters for zinc(II) hexanoate are compared with the single crystal data. Indeed, the values are almost identical as given in Table 4. Additionally, the single crystal lattice parameters are used to generate powder patterns, which are in excellent agreement with the experimentally derived one. Typical results of the refinements and comparison with experimental data are shown in Fig. 6 for ZnC₅, ZnC₁₂ and ZnC₂₀. The observed and experimental lines match to a high degree of accuracy. All the compounds crystallize in the monoclinic space group, as predicted by the infrared data, with P symme-

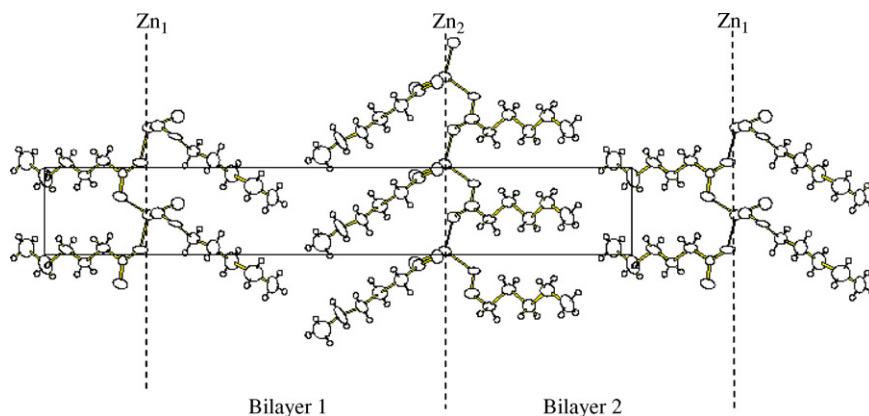
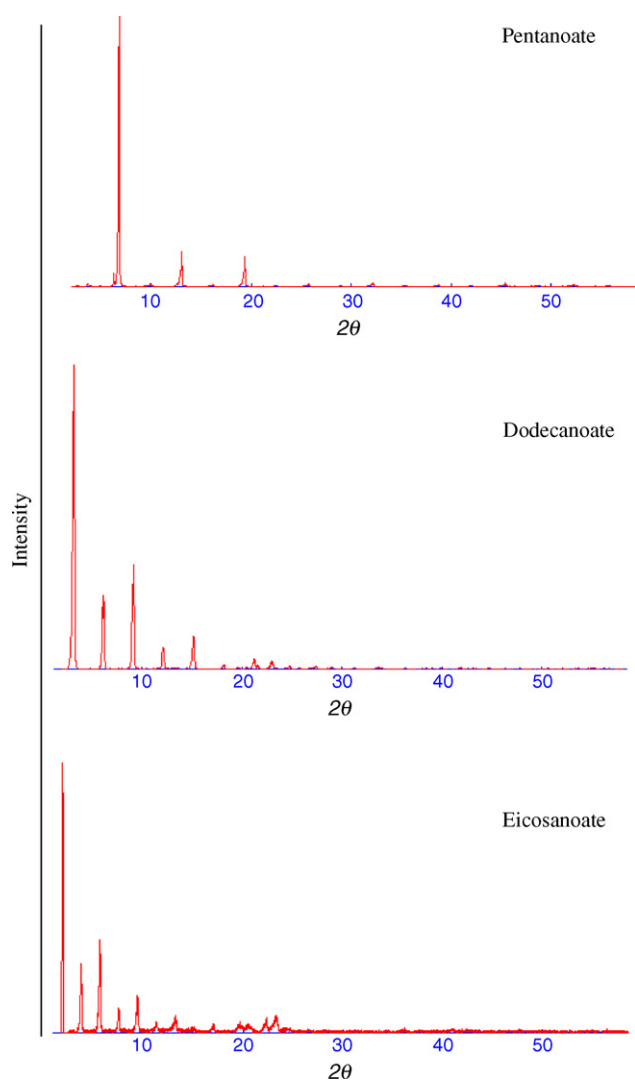
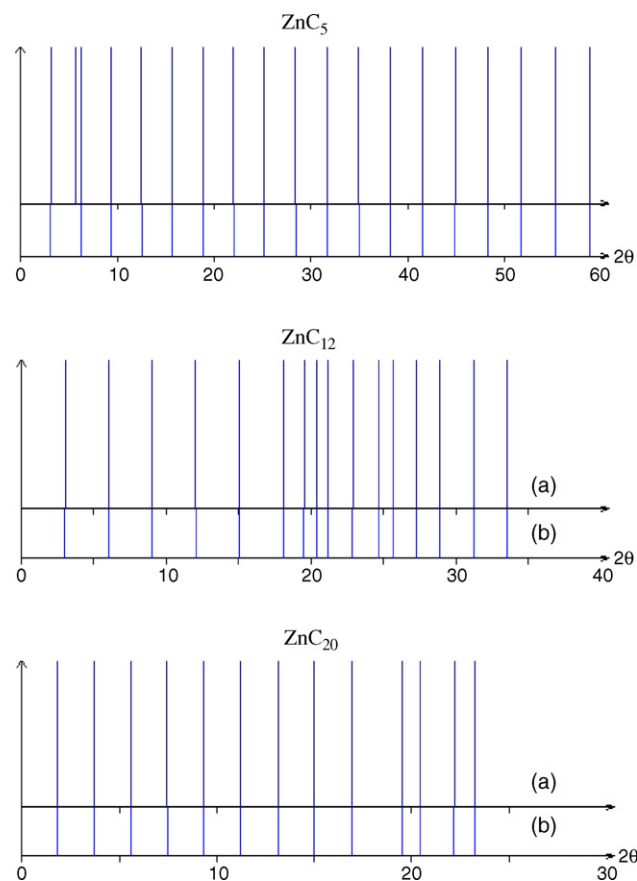


Fig. 4. Molecular projection of structure of zinc(II) hexanoate. Displacement ellipsoids drawn at 30% probability level.

Fig. 5. X-ray powder diffraction patterns for ZnC_5 , ZnC_{12} and ZnC_{20} .Fig. 6. Observed (a) and calculated (b) powder diffraction line patterns for ZnC_5 , ZnC_{12} and ZnC_{20} .

try (unfortunately, the powder method is not accurate enough to determine the precise space group). Lattice parameters are collected in Table 4 and a plot of the experimentally derived lamellae distances between two Zn(1) or Zn(2) planes, d_{exp} versus n_C shows a discontinuity at $n_C = 8$ (Fig. 7), which is also replicated in the plots of unit cell side a (the principal axis) and

Table 4
Powder X-ray data for zinc(II) n -alkanoates

Compound	a (Å)	b (Å)	c (Å)	β (°)	d_L (Å)	d_{exp} (Å)
ZnC_4	25.52	4.96	9.69	94.70	6.97	25.43
ZnC_5	28.26	4.99	9.04	90.13	8.24	28.26
ZnC_6	32.27 (32.31)	5.02 (4.71)	9.08 (9.33)	90.78 (93.72)	9.50	32.27
ZnC_7	36.54	5.31	10.31	97.53	10.76	36.22
ZnC_8	42.36	5.22	10.21	99.93	12.02	41.72
ZnC_9	24.40	6.02	9.12	92.85	13.28	24.38
ZnC_{10}	25.79	5.57	9.25	95.88	14.54	25.65
ZnC_{11}	28.05	5.50	9.47	95.23	15.80	27.93
ZnC_{12}	29.53	5.41	9.70	94.96	17.07	29.41
ZnC_{13}	31.45	5.62	9.48	93.54	16.33	31.39
ZnC_{14}	33.91	5.65	9.61	95.17	19.59	33.78
ZnC_{15}	36.69	5.42	9.58	95.63	20.85	36.52
ZnC_{16}	38.36	5.50	9.39	94.93	22.11	38.21
ZnC_{17}	40.95	5.49	9.50	94.80	23.37	40.81
ZnC_{18}	42.67	5.50	9.09	93.66	24.64	42.58
ZnC_{19}	45.18	5.64	8.99	91.93	25.90	45.16
ZnC_{20}	47.27	5.54	9.09	93.09	27.16	47.20

The values in parentheses denotes single crystal data.

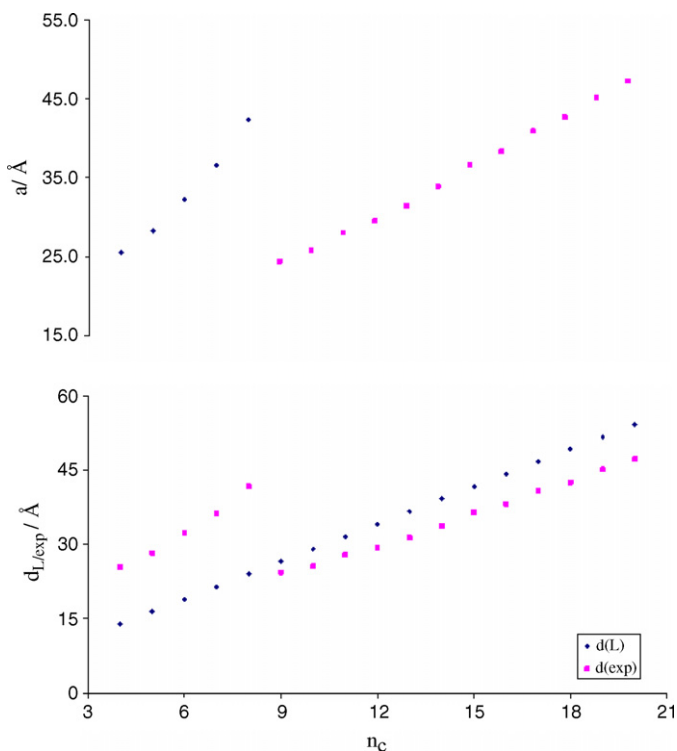


Fig. 7. Unit cell side, a (Å), molecular length (d_L) and experimental lamellar spacing, d_{exp} vs. n_C .

cell volume, V_{cell} versus n_C . However, sides b , c and angle, β remain fairly constant with increasing n_C . It is clear then that the packing arrangements of hydrocarbon chains in the lattice for $n_C \leq 8$ and $n_C \geq 9$ are different. To confirm this, d_{exp} values determined from 100 (hkl) reflections and calculated values, d_L determined from the fully extended all-trans configuration from the expression:

$$d_L = d_{C-H} + (n - 1)d_{C-C} \sin 55^\circ + d_{C-O} + r_{Zn}^{2+},$$

where n is the total number of carbon atoms, $d_{C-H} = 1.09$ Å, $d_{C-C} = 1.54$ Å, $d_{C-O} = 1.36$ Å and $r_{Zn}^{2+} = 0.74$ Å, are compared. An examination of the data shows that for $n_C \leq 8$, there are four hexanoate ligands (a double bilayer) within the zinc basal plane. Side chain interactions are not strong since in the region in which they predominate, in the powder trace, very few weak reflections are observed. For longer chain lengths, $n_C \geq 9$ a bilayer is indicated. Since $2d_L$ is greater than d_{exp} , an interdigitated in-plane–in-plane lattice model is proposed for these homologues. In support of this, several low intensity lines are observed in the side chain interaction region of the powder trace. Moreover, both models are consistent with the data presented in Table 5, where there are two molecules ($Z=2$) within the unit cell for $n_C \leq 8$ and one ($Z=1$) for the longer chain homologues. Such a difference in structure between the short and long chains can be visualized in two-dimensional structural propagations. In the short chain length structures, the carboxylate groups above the zinc layer form bidentate bridges between zinc centres and have a zig-zag arrangement that is in the plane of the page, whereas below the zinc layer the chains have a zig-zag arrangement that is perpendicular to the page. Such a depiction might explain the

Table 5

Cell volume, V_{cell} , tilt angles, r ($^\circ$) and number of molecules in a unit cell, Z for zinc(II) n -alkanoates

Compound	V_{cell} (Å ³)	r ($^\circ$)	Z
ZnC ₄	1222.79	55.80	2
ZnC ₅	1275.09	58.86	2
ZnC ₆	1472.42	58.13	2
ZnC ₇	1982.09	57.39	2
ZnC ₈	2225.19	60.19	2
ZnC ₉	1339.03	66.62	1
ZnC ₁₀	1322.10	61.89	1
ZnC ₁₁	1468.46	62.04	1
ZnC ₁₂	1541.98	59.48	1
ZnC ₁₃	1674.22	58.9	1
ZnC ₁₄	1833.71	59.51	1
ZnC ₁₅	1895.51	61.14	1
ZnC ₁₆	1977.51	59.78	1
ZnC ₁₇	2127.90	60.82	1
ZnC ₁₈	2128.63	59.77	1
ZnC ₁₉	2291.00	60.67	1
ZnC ₂₀	2375.94	60.33	1

perpendicular cleavage planes observed under polarized light. The longer chain length structures, for which an interdigitated bilayer arrangement is proposed, are packed differently, with a head-to-tail arrangement of hydrocarbon chains within the lattice. Such an arrangement should lead to side chain interactions in the long chain compounds, which are indeed seen in the powder traces. Hence, the structural models previously proposed [1] must be modified, somewhat, in light of these results (Fig. 2).

References

- [1] R.A. Taylor, H.A. Ellis, P.T. Maragh, N.A.S. White, *J. Mol. Struct.* 787 (2006) 113.
- [2] W. Clegg, I.R. Little, B.P. Straughan, *Acta Cryst. C* 42 (1986) 1701.
- [3] T. Ishioka, Y. Shibata, M. Takahashi, T. Kanesaka, *Spectrochim. Acta* 54 (1998) 1811.
- [4] E. Goldschmied, A.D. Rae, N.C. Stephenson, *Acta Cryst. B* 33 (1977) 2117.
- [5] N. Segedin, Z.M. Lah, I. Leban, L. Golic, *Acta Chim. Slov.* 46 (1999) 173.
- [6] I. Ishioka, K. Maeda, I. Watanabe, S. Kawauchi, M. Harada, *Spectrochim. Acta A* 56 (2000) 1731.
- [7] J. Blair, R.A. Howie, J.L. Wardell, *Acta Cryst. C* 49 (1993) 219.
- [8] W. Clegg, I.R. Little, B.R. Straughan, *Acta Cryst. C* 43 (1987) 456.
- [9] J. Peultier, M. Francois, J. Steinmetz, *Acta Cryst. C* 55 (1999) 2064.
- [10] F. Lacouture, J. Peultier, M. Francois, J. Steinmetz, *Acta Cryst. C* 56 (2000) 556.
- [11] Bruker, Xscans, SHELXTL (Version 5.1), Bruker AXS Inc., Madison, WI, USA, 1997.
- [12] G.M. Sheldrick, SHELXS 97 and SHELXL 89, Programmes for the Solution and Refinement of Crystal Structures from Diffraction Data, University of Göttingen, Germany, 1997.
- [13] L.J. Farrugia, ORTEP-3 for Windows, *J. Appl. Cryst.* 30 (1997) 565.
- [14] M.E. Ekwunife, M.U. Nwachukwu, F. Rinehart, S.J. Sime, *J. Chem. Soc. Faraday* 71 (1975) 1432.
- [15] P. Ferloni, E.S. Westrum Jr., *Pure Appl. Chem.* 64 (1992) 73.
- [16] R. Boese, H.C. Weiss, D. Blaser, *Angew. Chem. Int. Ed. Engl.* 38 (1999) 988.
- [17] V.R. Thalladi, R. Boese, H.C. Weiss, *J. Am. Chem. Soc.* 122 (2000) 1186.
- [18] K. Nakamoto, *Infrared Spectra of Inorganic and Coordination Compounds*, Wiley, New York, 1963, p. 198 (et seq).
- [19] G.D. Deacon, R.J. Phillips, *Coord. Chem. Rev.* 33 (1980) 227.

- [20] K. Nakamoto, P.J. McCarty, *Spectroscopy and Structure of Metal Chelate Compounds*, Wiley, New York, 1963, p. 268 (et seq).
- [21] K.N. Mehrotra, R. Kachwaha, M. Sing, *Thermochim. Acta* 62 (1983) 179.
- [22] M.A. Mesubi, *J. Mol. Struct.* 81 (1982) 61.
- [23] N.W. Alcock, V.M. Tracy, T.C. Waddington, *J. Chem. Soc. Dalton Trans.* (1976) 2243.
- [24] H.A. Ellis, N.A.S. White, I. Hassan, R. Ahmad, *J. Mol. Struct.* 738 (2005) 71.
- [25] K.C. Patil, G.V. Chandrashakhar, M.V. George, N.R. Rao, *Can. J. Chem.* 46 (1967) 257.
- [26] R.G. Snyder, *J. Mol. Spectrosc.* 7 (1961) 116.
- [27] H.A. Ellis, *Mol. Cryst. Liq. Cryst.* 139 (1986) 281.
- [28] H.A. Ellis, A. de Vries, *Mol. Cryst. Liq. Cryst.* 163 (1988) 133.